Elastic and inelastic scattering for the ^{11}B + ^{58}Ni system: Target and projectile reorientation effects

N. N. Deshmukh,[1] V. Guimarães,[1,2] E. Crema,[1] D. Abriola,[3] A. Arazi,[3,4] E. de Barbará,[3] O. A. Capurro,[3] M. A. Cardona,[3,4] J. Gallardo,[3,4] D. Hojman,[3,4] G. V. Martí,[3] A. J. Pacheco,[3,4] D. Rodrígues,[3,4] Y. Y. Yang,[1,5] A. N. Deshmukh,[1] D. R. Mendes Jr.,[6] V. Morcelle,[7] V. Scarduelli,[1] and D. S. Monteiro[8]

[1]*Instituto de Física, Universidade de São Paulo, Caixa Postal 66318, São Paulo 05315-970, São Paulo, Brazil*
[2]*Institut de Physique Nucleaire d'Orsay, UMR8608, IN2P3-CNRS, Université Paris Sud 11, 91406 Orsay, France*
[3]*Laboratorio TANDAR, Comisión Nacional de Energía Atômica, B1650KNA San Martín, Buenos Aires, Argentina*
[4]*Consejo Nacional de Investigaciones Científica y Técnicas, Avenue Rivadavia 1917, C1033AAJ Buenos Aires, Argentina*
[5]*Institute of Modern Physics, Chinese Academy of Sciences, Lanzhou 730000, China*
[6]*Instituto de Física, Universidade Federal Fluminense, Avenida Litoranea s/n, Gragoatá, Niterói, 24210-340 Rio de Janeiro, Brazil*
[7]*Departament of Physics, Universidade Federal Rural do Rio de Janeiro, Seropédica, 23890-000 Rio de Janeiro, Brazil*
[8]*Universidade Federal da Integração Latino-Americana, Instituto Latino-Americano de Ciências da Vida e da Natureza, Foz do Iguaçu, Paraná, Brazil*

(Received 2 September 2015; published 20 November 2015)

Full angular distributions for elastic and inelastic scattering of ^{11}B on ^{58}Ni have been measured at different bombarding energies around the Coulomb barrier. Measurement and analysis with coupled-channel calculations have been performed for the first time for a system with the tightly bound ^{11}B as projectile on a medium mass target. In these calculations, the real part of the interaction potential between nuclei was represented by a parameter-free double-folding potential. To avoid the use of an imaginary potential at the surface, several inelastic transitions of the projectile and the target have been included in the coupling matrix. The result of these coupled-channel calculations are in very good agreement with all experimental angular distributions. The most important result was the striking influence on the reaction mechanism of the ground-state-spin reorientation of the ^{11}B nuclei.

DOI: 10.1103/PhysRevC.92.054615 PACS number(s): 25.70.Bc, 24.10.Eq

I. INTRODUCTION

Elastic scattering is the simplest process which can occur in the collision of two nuclei. At low energies, it is a surface process and thus very suitable to investigate surface properties such as deformations and cluster configuration. It is already well known that large-angle elastic and inelastic scattering between light- and heavy-ion partners depends on the structure of the interacting nuclei through their single-particle or collective configurations. For instance, a large contribution in the elastic scattering is expected from the nonspherical part of the matter distribution of nuclei that had large ground-state quadrupole moments. The effect of the quadrupole moment, which can be as large as the total inelastic cross sections, is to fill the back-angle minima in the elastic differential cross sections [1]. Spin-orbit terms can be small but can increase the back-angle structure in the angular distributions [2], competing with the dumping effect of the quadrupole moment. Elastic scattering measurements for the ^{11}B + ^{27}Al [3] and ^{11}B + ^{16}O [1] systems have shown the importance of including quadrupole terms in the elastic scattering potential to describe the data. Also, the significant back-angle differences in the elastic differential cross sections for ^{10}B and ^{11}B + ^{27}Al of data [3] were attributed mainly to the quadrupole moments, although the authors did not rule out the possibility of spin-orbit effect. This was later specifically investigated by Petrovich *et al.* and they concluded that no such effect was observed in the potentials for ^{10}B and ^{11}B + ^{27}Al systems [4]. Another important effect is the ground-state target-spin reorientation, which has already been observed in the diffraction minima in the elastic scattering of light particles by odd-mass targets [5,6]. In this sense, scattering of the ^{11}B, which is an odd nucleus, on an even-mass target is an interesting system to investigate the combination of spin-orbit and quadrupole effects. The ^{11}B nucleus has a nonzero ground-state deformation, $Q = +0.0407\ b$, and a negative parity spin, $J^{\pi} = 3/2^{-}$, indicating a nonspherical symmetric charge distribution. It is also a strongly bound nucleus with binding energy of 8.67 MeV in respect to the ^{7}Li + α channel decay and with many bound excited states.

More recently, it has been observed that the ground-state reorientation process plays a dominant role in the elastic scattering of ^{11}B by light targets at large angles [7,8]. Elastic scattering measurements with even-mass target nuclei has also shown some target reorientation effects [9]. It is important to mention that in these previous works on ^{11}B elastic scattering, where reorientation has been taken into account, only a few states were included in the coupling calculations and thus, to compensate for the absence of many states, an imaginary potential had been used. The reorientation effects in the elastic scattering are in the direction of reducing the strength of the optical model imaginary potential. Rather, if all important states in the coupling matrix are included, there will be no need to consider an imaginary potential at the surface.

In the present work, new data for the elastic and inelastic scattering of ^{11}B ions by ^{58}Ni target at several energies close to the Coulomb barrier are reported. These new data were analyzed with a parameter-free coupled-channel calculation (CCC). In this approach, the real part of the interaction

 ©2015 American Physical Society

potential is represented by the parameter-free double-folding Sao Paulo potential (SPP) [10]. No imaginary potential at the interaction region was employed since as many reaction channels as possible were included in the coupling scheme. It is important to stress that within such an approach, we are not fitting data by varying a lot of potential parameters, and the theoretical results can just be compared to data. Among the inelastic channels investigated, we were particularly interested in the spin reorientations of the projectile ^{11}B as well as for the ^{58}Ni target.

Another motivation for the present work on the elastic scattering of $^{11}\mathrm{B} + {}^{58}\mathrm{Ni}$ is the possibility to further investigate the systematic of the scattering between members of an isotopic chain of Boron projectiles involving tightly bound, stable–weakly bound, and radioactive-halo nuclei on the same target. Data on elastic scattering for $^{8}\mathrm{B} + {}^{58}\mathrm{Ni}$ system are already available in the literature [11], data on $^{10}\mathrm{B} + {}^{58}\mathrm{Ni}$ system are being analyzed [12], while measurement of $^{12}\mathrm{B} + {}^{58}\mathrm{Ni}$ system is being proposed by our group.

In Sec. II we describe the details of the experiment. In Sec. III we present the coupled-channels calculations and the comparison of the results with the data. Finally, we give the summary and derive main conclusions in Sec. IV.

II. EXPERIMENTAL SETUP AND MEASUREMENTS

The experiment was performed using ^{11}B stable beam from the 20 UD tandem accelerator at the Tandar laboratory in Buenos Aires, Argentina. The elastic scattering angular distributions were measured for ^{11}B beam at seven different bombarding energies below and above the Coulomb barrier, namely, $E_{\mathrm{Lab}} = 19.0$, 20.0, 21.0, 23.0, 24.0, 25.0, and 35.0 MeV, which in the center of mass frame corresponds to $E_{\mathrm{c.m.}} = 15.97$, 16.81, 17,65, 19.33, 20.17, 21.01, and 29.41 MeV. The nominal Coulomb barrier for this system in the laboratory frame is around 23 MeV. Beam intensity ranged from 3 to 10 pnA. The beam was bombarded on the enriched (99.84%) ^{58}Ni target. We used two targets; one of them was 100 μg/cm^2 thick and with a very thin layer of evaporated ^{197}Au with nominal thickness of 12 μg/cm^2, and the other was 124 μg/cm^2 thick with also a very thin ^{197}Au layer, 20 μg/cm^2 thick. For the measurements at energies $E_{\mathrm{c.m.}} = 15.97$, 16.81, 20.17, 21.01, and 29.41 MeV the 112-μg/cm^2-thick target was used, while for $E_{\mathrm{c.m.}} = 17.65$ and 19.33 MeV the 144-μg/cm^2-thick target was used. The energies considered in the analysis were the energies in the half-target thickness, which for these thin target, a correction of about 100 keV was required. The detection system used for the measurements consisted of an array of eight planar silicon surface-barrier detectors, 150 μm thick, with an angular separation of 5° between adjacent detectors. These detectors were mounted in a 70-cm-diameter scattering chamber. More details about the detector and the data-acquisition systems can be found in Ref. [13]. Two separate silicon surface-barrier detectors were kept fixed at the most backward angles of 160.0° and 168.1° for all measurements. Two monitors, silicon detectors, were placed at forward angles ±16.0° related to the beam direction for the absolute normalization purpose. In subsequent runs, the ^{11}B beam was used to bombard a separate

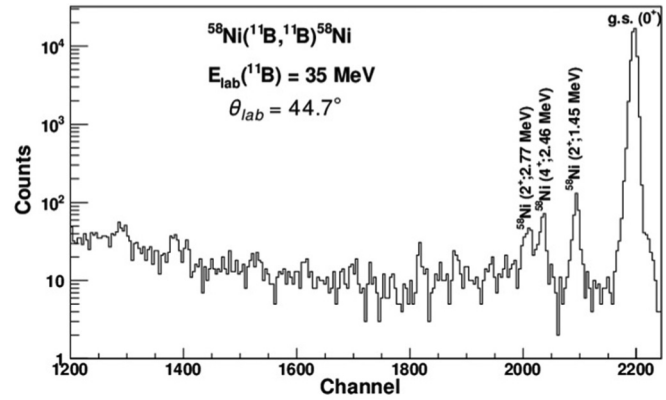

FIG. 1. Typical energy spectra for the $^{11}\mathrm{B} + {}^{58}\mathrm{Ni}$ system measured at $\theta_{\mathrm{Lab}} = 44.7°$ and $E_{\mathrm{c.m.}} = 29.41$ MeV. The contributions of the excited states ^{58}Ni (2^+, 4^+, 2^+) are indicated.

^{197}Au target, 150 μg/cm^2 thick, for calibration purpose and also to accurately obtain the solid angle ratio between each detector and the monitors. The solid angles subtended by the array of eight detectors, the two backward detectors, and the two monitors were 0.285, 0.123, 0.193, 0.285, 0.296, 0.383, 0.561, 0.696, 0.709, 0.799, 0.020, and 0.020 msr, respectively. The equivalent angular openings were in the range of 0.3° to 0.8°. The angular distributions were measured at angles from 27.0° to 172.2°, at lower energies, and from 27.0° to 125.2° for higher energies. The absolute uncertainties in the cross sections ranged from 0.3% to 8% starting from most forward to most backward angles for the lower energies and 0.2% to 27% for the highest energy of $E_{\mathrm{c.m.}} = 29.41$ MeV. A very small contribution from target contaminants such as carbon, oxygen, and silicon were observed and accurately estimated, thanks to the good calibration performed for each detector. Contributions from the inelastic-scattering channels were determined for the first 2^+ excited state of the ^{58}Ni nucleus ($E^* = 1.4542$ MeV), at the lower energies, and for the most backward angles. For the highest energy measurement, well-defined peaks of the three excited states of ^{58}Ni nucleus (2^+, 4^+, and 2^+ at $E^* = 1.454$, 2.459, and 2.775 MeV, respectively) were observed and taken into account. An energy spectrum showing these inelastic contributions, measured at laboratory angle of 44.7°, is presented in Fig. 1. The experimental resolution and good calibration allowed their identification and separation.

III. COUPLED-CHANNELS CALCULATIONS

Nowadays, a more physically satisfying approach to analyze elastic scattering data is achieved by performing explicit coupled-channels calculations, where a parameter-free real potential is used and the most (if not all) dominant reaction channels are included, which avoids the use of imaginary potential at surface [15,16]. This approach has more physical meaning than fitting data with six-parameter Woods-Saxon potentials, and it is very appropriate to take into account the nonelastic channels, especially the ones arising from collective excitations. This is also a particularly powerful approach to

perform simultaneous analysis of elastic, inelastic, and fusion processes. In the present work we performed a simultaneous analysis of elastic and inelastic channels. In a coupled-channel calculation it is necessary to consider a bare potential to simulate the nuclear interaction between projectile and target nuclei, whereas the energy-dependent polarization potential, which takes into account the nonelastic channels, is generated implicitly from the couplings. In the present work we represent the bare interaction by the parameter-free double-folding Sao Paulo potential (SPP) [10]. It has already been demonstrated that this double-folding potential can be considered a reliable starting point for CCC even for systems with unstable nuclei [14]. For the energy range of the present investigation (near the Coulomb barrier) the SPP is almost energy independent, and the relevant feature for the calculations is its double-folding characteristic. We then followed the procedure adopted in the works of Refs. [15] and [16], which consists of using a short-range imaginary potential to simulate the absorption of flux due to fusion (as the fusion is not explicitly included in the calculation). The important point of this approach, which should be emphasized, is the absence of any imaginary potential at the interaction surface region. This means that a large number of reaction channels needs to be included in the coupling matrix and, consequently, any surface imaginary potential should be excluded to avoid double counting in the calculations. For the short-range imaginary potential, which takes into account the absorption by the fusion process, we used a fixed Woods-Saxon shape potential with the parameters: $V_i = 80$ MeV, $r_i = 0.9$ fm, and $a_i = 0.5$ fm. The final results are not very sensitive to this particular choice of parameters. In conclusion the calculation is parameter free and the results were directly compared to data. All the calculations, described in more detail in the next sections, were performed using the code FRESCO [17].

TABLE I. Spin parity and energy of the states in ^{58}Ni and ^{11}B, from the NNDC database [18], considered in the coupled-channel calculations.

^{58}Ni		^{11}B	
J^π	E (MeV)	J^π	E (MeV)
0^+	g.s.	$3/2^-$	g.s.
2^+	1.4542	$5/2^-$	4.4444
4^+	2.4592	$3/2^-$	5.0203
2^+	2.7754	$7/2^-$	6.7418
0^+	2.9425		
2^+	3.0378		
2^+	3.2636		
3^+	3.4205		
0^+	3.5311		
4^+	3.6200		
3^+	3.7750		
2^+	3.8988		
2^+	4.1084		
4^+	4.2947		
4^+	4.4043		
0^+	4.5380		

A. Elastic scattering angular distribution with the coupling effects

We analyzed the angular distribution for the elastic scattering of ^{11}B + ^{58}Ni at several energies around the Coulomb barrier with coupled-channel calculation as described in the previous sections. To investigate the effect of each reaction channel and the interference between them on the reaction dynamic of this system, we added in the coupled scheme, one by one, the relevant channels. In particular, we considered inelastic states and reorientation effects. The calculated cross sections for each coupled channel were compared to the experimental data for each angular distribution. The spin, parity, and energy of the excited states for both ^{11}B and ^{58}Ni included in the calculations are listed in Table I. Almost all nuclear transitions with experimental $B(E2)$ and $B(E3)$ values available in the literature [18] for the projectile and target were considered in the calculation, and these values are listed in Table II. In the present CCC, the excited states were considered to be collective in nature, and the transitions with no change in parity were calculated within the rotational model.

In Figs. 2(a) and 2(b) we show the detailed comparison of calculated cross sections to the experimental data obtained at $E_{\text{c.m.}} = 21.01$ MeV, where the cumulative effect of the opening of reaction channels are straightforwardly distinguished. In Fig. 2(a) we show the cross sections in linear scale, while

TABLE II. All inelastic transitions for ^{58}Ni and ^{11}B used in the coupled-channel calculations.

		^{58}Ni		
$I_f \leftrightarrow I_i$	E_γ (KeV)	$B(E2)$ (W.u.)	$\langle I_f \vert E_\gamma \vert I_i \rangle$ (e^2 fm^4)	δ_2 (fm)
$0 \leftrightarrow 2$	1454.28	10.0	25.822	0.9410
$2 \leftrightarrow 4$	1004.80	11.2	36.664	1.3361
$2 \leftrightarrow 2$	1321.2	15.0	31.626	1.1525
$0 \leftrightarrow 2$	2775.5	0.029	1.391	0.0507
$2 \leftrightarrow 0$	167.2	21.0	16.735	0.6098
$2 \leftrightarrow 0$	1488.3	0.0004	0.073	0.0027
$2 \leftrightarrow 2$	262.6	5.0	18.259	0.6654
$2 \leftrightarrow 2$	1583.8	1.8	10.956	0.3992
$0 \leftrightarrow 2$	3037.7	1.15	8.757	0.3191
$2 \leftrightarrow 2$	1809.5	8.0	23.096	0.8417
$0 \leftrightarrow 2$	3263.4	1.9	11.256	0.4102
$2 \leftrightarrow 3$	382.9	7.0	25.563	0.9315
$4 \leftrightarrow 3$	961.0	0.07	2.556	0.0932
$2 \leftrightarrow 0$	2076.9	5.6	8.642	0.3149
$2 \leftrightarrow 4$	2166.3	1.3	12.491	0.4552
$4 \leftrightarrow 3$	1316.4	0.8	8.642	0.3149
$0 \leftrightarrow 2$	3898.0	0.5	5.774	0.2104
$2 \leftrightarrow 2$	2654.6	0.26	4.164	0.1517
$0 \leftrightarrow 2$	4107.4	0.13	2.944	0.1073
$2 \leftrightarrow 4$	2840.8	6.0	26.835	0.9779
$2 \leftrightarrow 4$	1923.9	4.4	22.981	0.8374
$2 \leftrightarrow 0$	3083.7	4.9	8.084	0.2946
		^{11}B		
$3/2 \leftrightarrow 5/2$	4444.03	6.10	7.293	2.5903
$1/2 \leftrightarrow 3/2$	2895.30	40.00	15.248	5.4160
$3/2 \leftrightarrow 3/2$	5018.98	0.57	1.820	0.6465
$3/2 \leftrightarrow 7/2$	6739.53	1.26	3.827	1.3594

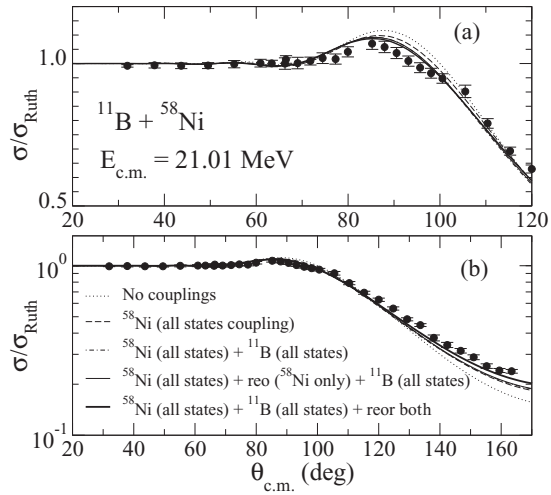

FIG. 2. Elastic scattering angular distribution for the ^{11}B + ^{58}Ni system at $E_{c.m.} = 21.01$ MeV in (a) linear and (b) logarithmic scales. The lines are results of coupled-channel calculations. See text for details.

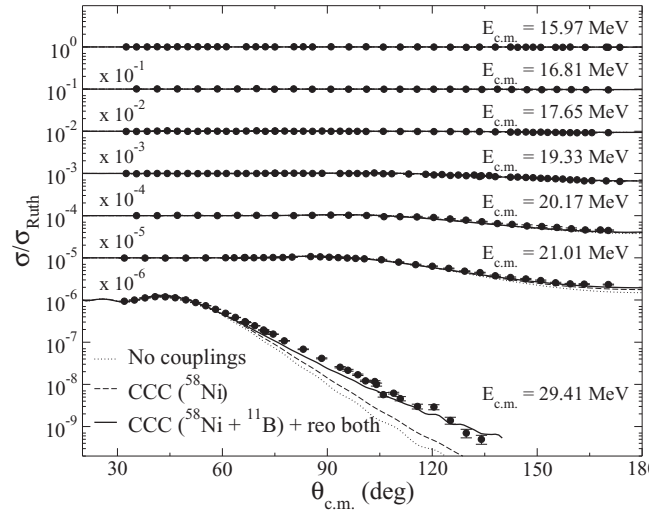

FIG. 3. Elastic scattering angular distributions for the ^{11}B + ^{58}Ni system at $E_{c.m.} = 15.97$, 16.81, 17.65, 19.33, 20.17, and 29.41 MeV. The lines represent the CC calculations as indicated: dotted line is without any couplings, dashed lines couplings are only the target excited states, and solid lines are the full CCC including the reorientations for both target and projectile.

in Fig. 2(b) the same angular distribution is shown in logarithmic scale. The idea of plotting in different scales is to emphasize and disentangle the results in the different angular regions, especially at the grazing and at backward angles. In these figures, the dotted line is the prediction of the CCC when all the reaction channels are closed; the dashed line represents the results when coupling all states of the target; the dashed-dotted line corresponds to the calculation where all the excited states of both target and projectile are included in the coupling matrix. The thin solid line shows the effect when the reorientation channel is included for the first excited state of target and, finally, the thick solid line is when the ground-state reorientation channel for the projectile was included. As can be qualitatively observed in the figures, the coupling effect of all channels on the reaction mechanism is the same, deviating the elastic flow from forward angles to backward angles. The coupling of all excited states of the target (dashed line) has a large impact on the elastic cross sections. However, this effect is mainly due to the first excited state of ^{58}Ni(2^+). On the other hand, as shown by the dashed-dotted line, the excited states of the projectile have a smaller influence as compared to the target ones. The thin solid line shows that the spin reorientations of the exited states of the target have very little influence on the coupling final result. Nevertheless, a remarkable influence on the entire reaction mechanism was observed when the reorientation of the ^{11}B ground state was included in the calculation (thick solid line in Fig. 2). As mentioned before, the same phenomena was recently observed with lighter targets [7,8]. It would be interesting to investigate if this effect appears when a target heavier than ^{58}Ni is used.

The coupled-channel calculations were extended to all the other six elastic angular distributions, namely at energies $E_{c.m.} = 15.97$, 16.81, 17.65, 19.33, 20.17, and 29.41 MeV. The results of such calculations are compared to data in Fig. 3. In this figure the dotted lines represent the calculations performed without any couplings, the dashed lines correspond to calculation where only the target excited states were coupled, and the solid lines are the full CCC where all reorientation channels and projectile transitions were included in the coupling scheme. As can be seen, very good agreement between calculations and data is achieved for all energies. In all energies investigated in this work the reorientations of the excited states of the target have minor importance. The angular distribution at 29.41 MeV indicates that the coupling of the projectile inelastic channels has stronger influence on the final result than the target channels. An inverse result was observed at 21.01 MeV, where the target channels has more influence. It means that the relative importance between the projectile and target states on the reaction mechanism has increased with the bombarding energy. This result should be investigated in a wider energy range. Finally, we emphasize once more that these calculations are parameter free and no artificial superficial imaginary potential has been used. In this approach, the absorption from the elastic channel is produced by the real process of opening inelastic channels.

B. Inelastic scattering angular distributions

An important test of the self-consistency of the coupled-channel calculations is to compare the results of the calculated inelastic cross sections with the data. Such comparison is presented in Fig. 4. Six angular distributions for the inelastic scattering of the target first excited state, ^{58}Ni (2^+, 1.454 MeV) have been measured at $E_{c.m.} = 15.97$, 16.81, 17.65, 19.33, 20.17, and 21.01 MeV. As can be seen, this parameter-free calculation agrees very well with data for all energies measured. Even the small oscillations in

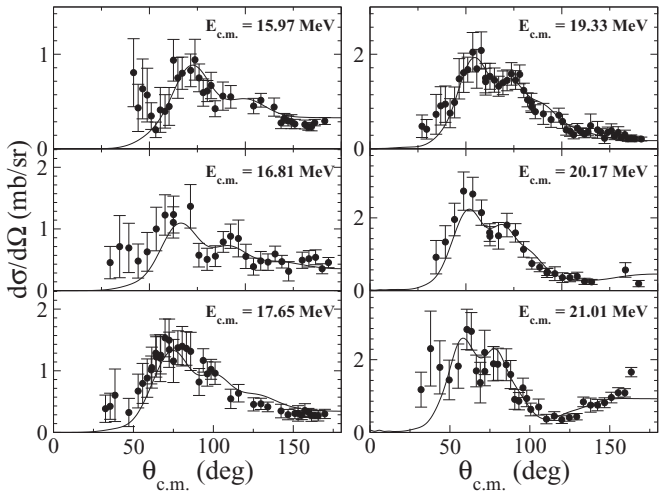

FIG. 4. Inelastic scattering angular distributions for the ^{11}B + ^{58}Ni (2^+, 1.454) first excited state measured at $E_{\text{c.m.}} = 15.97$, 16.81, 17.65, 19.33, 20.17, and 21.01 MeV. The solid lines are the results of the CC calculations.

all angular distributions were predicted by our theoretical approach.

Finally, as the inelastic angular distributions for the first, second, and third excited states of the target, ^{58}Ni (2^+, 4^+, 2^+), could be measured at the highest energy studied ($E_{\text{c.m.}} = 29.41$ MeV), it was possible to perform an even more rigorous test of our calculations. Figure 5 shows the comparison of the theoretical predictions and data for these inelastic angular distributions, where an excellent agreement can be observed. In conclusion we can say that with the present parameter-free calculation we were able to predict simultaneously all experimental data measured and presented in this work.

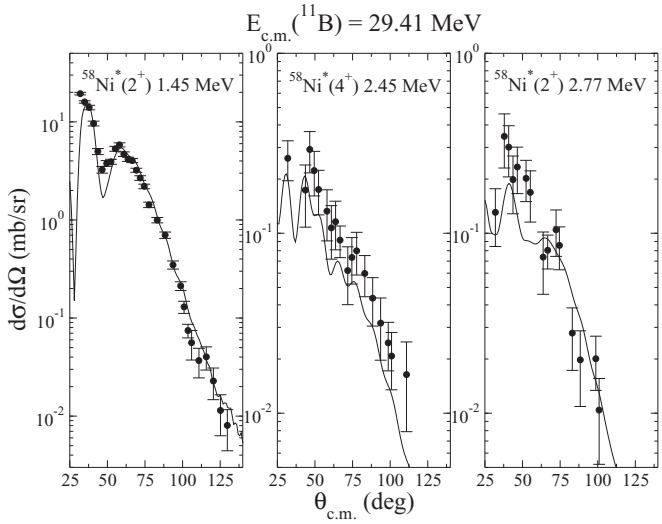

FIG. 5. Inelastic scattering angular distributions for the ^{11}B + ^{58}Ni (2^+, 4^+, 2^+) first, second, and third excited states measured only at $E_{\text{c.m.}} = 29.41$ MeV. The solid lines are the results of the CC calculations.

At last, it should be mentioned that no well-defined evidence of transfer channel events was found in our spectra, which means the transfer cross section are much smaller than the inelastic ones at the energies around the Coulomb barrier investigated in this work. Besides, as has been shown above, the data were well described by coupled-channel calculations without including any transfer channels, indicating that these channels have little influence in the reaction mechanism of this system at low bombarding energies.

IV. SUMMARY AND CONCLUSIONS

We have measured full angular distributions for elastic and inelastic scattering of ^{11}B on ^{58}Ni at different bombarding energies around the Coulomb barrier. Elastic scattering of ^{11}B has been measured for the first time on medium mass target. The inelastic scattering angular distributions from the first excited state of the ^{58}Ni target for all the energies, and three excited states for the highest energy, i.e., $E_{\text{c.m.}} = 29.41$ MeV, were measured. The measured angular distributions have been analyzed with coupled-channel calculations (CCC) including all the relevant excited states of projectile and target available in the literature. Our theoretical approach used the parameter-free double-folding Sao Paulo potential as the real bare potential and no imaginary potential at the surface, providing a free-parameter coupled-channel calculation. This approach was able to give a very good simultaneous description of the elastic and inelastic data. Among the several channels investigated, the ^{11}B ground-state spin reorientation and the ^{58}Ni first excited state had a striking influence on the reaction mechanism.

Our study shows the importance of elastic and inelastic scattering as a dominant way to understand the key role of the target-projectile effects on the nuclear reaction mechanism at energies in the vicinity of the Coulomb barrier. The fusion was included in the calculation by considering a very short-range imaginary potential. It would be interesting to have a measurements of fusion cross sections for this system for further comparison between fusion, elastic, and inelastic data, as well as to compare with the already measured fusion cross section for ^{8}B + ^{58}Ni [19]. This measurement will allow a systematic investigation of the scattering between members of an isotopic chain of boron projectiles involving tightly bound, stable–weakly bound, and radioactive-halo nuclei on the same target, since data on ^{8}B + ^{58}Ni are already available in the literature [11] and data on ^{10}B + ^{58}Ni are being analyzed [12].

ACKNOWLEDGMENTS

The author V.G. would like to thanks the São Paulo Research Foundation (FAPESP) (Grant 2014/14432-2) and the Conselho Nacional de Desenvolvimento Científico (CNPq) (Grant 302969/2013-6) for the financial support. The author N.N.D. thanks FAPESP (Grant 2012/17741-0) for the financial support. E.C. also thanks FAPESP and CNPq, and V.M. thanks FAPERJ for financial support.

[1] L. A. Parks, D. P. Stanley, L. H. Courtney, and K. W. Kemper, Phys. Rev. C **21**, 217 (1980).
[2] L. T. Chua, F. D. Becchetti, J. Janecke, and F. L. Milder, Nucl. Phys. A **273**, 243 (1976).
[3] L. A. Parks, K. W. Kemper, A. H. Lumpkin, R. I. Cutler, L. H. Harwood, D. Stanley, P. Nagel, and F. Petrovich, Phys. Lett. B **70**, 27 (1977).
[4] F. Petrovich, D. Stanley, L. A. Parks, and P. Nagel, Phys. Rev. C **17**, 1642 (1978).
[5] G. R. Satchler and C. B. Fulmer, Phys. Lett. B **50**, 309 (1974).
[6] S. E. Hicks and M. T. McEllistrem, Nucl. Phys. A **468**, 372 (1987), and references therein.
[7] S. Yu. Mezhevych *et al.*, Eur. Phys. J. A **50**, 4 (2014).
[8] A. T. Rudchik *et al.*, Nucl. Phys. A **939**, 1 (2015).
[9] F. Videbaek *et al.*, Nucl. Phys. A **256**, 301 (1976).
[10] L. C. Chamon, B. V. Carlson, L. R. Gasques, D. Pereira, C. De Conti, M. A. G. Alvarez, M. S. Hussein, M. A. Cândido Ribeiro, E. S. Rossi, Jr., and C. P. Silva, Phys. Rev. C **66**, 014610 (2002).
[11] E. F. Aguilera, E. Martinez-Quiroz, D. Lizcano, A. Gomez-Camacho, J. J. Kolata, L. O. Lamm, V. Guimarães, R. Lichtenthaler, O. Camargo, F. D. Becchetti, H. Jiang, P. A. DeYoung, P. J. Mears, and T. L. Belyaeva, Phys. Rev. C **79**, 021601(R) (2009).
[12] V. Scarduelli, V. Guimarães *et al.* (unpublished).
[13] D. Abriola *et al.*, Nucl. Instrum. Methods Phys. Res., Sect. B **268**, 1793 (2010).
[14] E. Crema, P. R. S. Gomes, and L. C. Chamon, Phys. Rev. C **75**, 037601 (2007).
[15] J. M. B. Shorto, E. Crema, R. F. Simões, D. S. Monteiro, J. F. P. Huiza, N. Added, and P. R. S. Gomes, Phys. Rev. C **78**, 064610 (2008).
[16] J. F. P. Huiza, E. Crema, D. S. Monteiro, J. M. B. Shorto, R. F. Simões, N. Added, and P. R. S. Gomes, Phys. Rev. C **75**, 064601 (2007).
[17] I. J. Thompson, Comp. Phys. Rep. **7**, 167 (1988).
[18] Evaluated Nuclear Structure Data Files, National Nuclear Data Center, Brookhaven National Laboratory, http://www.nndc.bnl.gov.
[19] E. F. Aguilera *et al.*, Phys. Rev. Lett. **107**, 092701 (2011).